Molecular Biology of the Cell
Vol. 17, 4709–4719, November 2006

Synaptic Vesicle Mobility and Presynaptic F-Actin Are Disrupted in a *N*-ethylmaleimide–sensitive Factor Allele of *Drosophila*[V]

Paula Nunes,* Nicola Haines,* Venkat Kuppuswamy,† David J. Fleet,† and Bryan A. Stewart*

Departments of *Biology and †Computer Science, University of Toronto, Mississauga, Ontario, Canada L5L 1C6

Submitted April 3, 2006; Accepted August 9, 2006
Monitoring Editor: Erika Holzbaur

***N*-ethylmaleimide sensitive factor (NSF) can dissociate the soluble NSF attachment receptor (SNARE) complex, but NSF also participates in other intracellular trafficking functions by virtue of SNARE-independent activity. *Drosophila* that express a neural transgene encoding a dominant-negative form of NSF2 show an 80% reduction in the size of releasable synaptic vesicle pool, but no change in the number of vesicles in nerve terminal boutons. Here we tested the hypothesis that vesicles in the NSF2 mutant terminal are less mobile. Using a combination of genetics, pharmacology, and imaging we find a substantial reduction in vesicle mobility within the nerve terminal boutons of *Drosophila* NSF2 mutant larvae. Subsequent analysis revealed a decrease of filamentous actin in both NSF2 dominant-negative and loss-of-function mutants. Lastly, actin-filament disrupting drugs also decrease vesicle movement. We conclude that a factor contributing to the NSF mutant phenotype is a reduction in vesicle mobility, which is associated with decreased presynaptic F-actin. Our data are consistent with a model in which actin filaments promote vesicle mobility and suggest that NSF participates in establishing or maintaining this population of actin.**

INTRODUCTION

N-ethylmaleimide–sensitive factor (NSF) was isolated on the basis of its ability to restore vesicle trafficking between Golgi membranes after treatment by *N*-ethylmaleimide (Block *et al.*, 1988). It was further shown that NSF can hydrolyze ATP and together with soluble NSF attachment protein (SNAP) this activity can dissociate the three-member protein complex known as the SNAP receptor (SNARE) complex (Whiteheart *et al.*, 1992; Sollner *et al.*, 1993a, 1993b; Whiteheart *et al.*, 1994). In addition to this established NSF function, other studies indicate that NSF likely has multiple cellular roles. These studies include reports of non-SNARE binding partners for NSF (Xu *et al.*, 1998; McDonald *et al.*, 1999; Han *et al.*, 2000; Cong *et al.*, 2001; Muller *et al.*, 2002; Martin *et al.*, 2006), and the role NSF plays in trafficking postsynaptic glutamate receptor subunits in the mammalian CNS (Nishimune *et al.*, 1998; Song *et al.*, 1998). Altogether, these data indicate that NSF is potentially central to many different types of intracellular trafficking events, some of which do not require SNARE proteins.

We have taken a genetic approach to studying NSF using the fruit fly, *Drosophila melanogaster*. *Drosophila* has two NSF genes, *comatose* (which encodes the NSF1 protein) and *NSF2* (Boulianne and Trimble, 1995; Pallanck *et al.*, 1995), whose proteins are 80% identical and are functionally redundant. NSF1 is the predominant functional isoform in the adult fly nervous system, although NSF2 is functionally important in other tissues and throughout development (Golby *et al.*, 2001). A null allele of *NSF2* dies as first instar larvae (Golby *et al.*, 2001), thus preventing examination of the easily accessible and widely studied third larval instar neuromuscular junction (NMJ). A dominant-negative NSF2 ($NSF2^{E/Q}$) transgene was generated by site-directed mutagenesis of a highly conserved amino acid within the D1 ATPase domain of the molecule (Stewart *et al.*, 2001), and the mutation renders a molecule that is capable of binding MgATP but it hydrolyzes ATP less well (Whiteheart *et al.*, 1994; Stewart *et al.*, 2001). When expressed in neurons, $NSF2^{E/Q}$ reduces synaptic strength, increases synaptic fatigue, and reduces size of the synaptic vesicle pool (Stewart *et al.*, 2002), consistent with previous work on NSF (Kawasaki *et al.*, 1998). Two unexpected findings emerged: first these changes occurred in the absence of detectable changes in SNARE complex abundance and second, the $NSF2^{E/Q}$ transgene induced a marked overgrowth of the neuromuscular junction.

Developmental and ultrastructural studies (Stewart *et al.*, 2005) further revealed that the $NSF2^{E/Q}$ induced overgrowth phenocopies an expanded NMJ found at the embryonic synapse of the $NSF2^{55}$ loss-of-function allele and that the larval $NSF2^{E/Q}$ NMJ has a reduced density of presynaptic active zones. Interestingly, there was no difference in the number of synaptic vesicles in the $NSF2^{E/Q}$ nerve terminal compared with controls. This suggests the reduction in vesicle pool size is not due to an endocytosis defect because genuine mutations of endocytotic genes all show dramatically reduced number of vesicles (Zhang *et al.*, 1998; Verstreken *et al.*, 2002, 2003; Koh *et al.*, 2004). To explain our data, we hypothesize that there is a

This article was published online ahead of print in *MBC in Press* (http://www.molbiolcell.org/cgi/doi/10.1091/mbc.E06–03–0253) on August 16, 2006.

[V] The online version of this article contains supplemental material at *MBC Online* (http://www.molbiolcell.org).

Address correspondence to: Bryan Stewart (bstewart@utm.utoronto.ca).

© 2006 by The American Society for Cell Biology

decrease in the intrabouton mobility of vesicles in the *NSF2$^{E/Q}$* nerve terminal.

MATERIALS AND METHODS

Fly Stocks

Drosophila melanogaster stocks were raised on Bloomington medium and crossed at room temperature or 25°C. *UAS-Actin-GFP* stocks were obtained from the Kyoto Stock Centre, *UAS-Synaptotagmin-GFP* (Zhang *et al.*, 2002) was obtained from the Bloomington Stock Center, and *UAS-moesin-GFP* flies were the gift of D. Kiehart (Edwards *et al.*, 1997). *elav-Gal4* is a pan-neuronal driver that expresses in postmitotic neurons. *elav^{c155}-Gal4* and *elav^{3A}-Gal4* lines were used to drive UAS gene expression in the control background. A recombinant third chromosome carrying *elav^{3A}-Gal4* and *UAS-NSF2$^{E/Q}$* is described in Stewart *et al.* (2002) and was used for *NSF2$^{E/Q}$* mutant experiments. We have previously shown that there is no effect of overexpressing wild-type *NSF2* and that *yw, UAS-NSF2$^{E/Q}$,* and *elav^{3A}-Gal4* are phenotypically equivalent with respect to NMJ overgrowth (Stewart *et al.*, 2002, 2005). Unless otherwise stated, larvae resulting from a cross of *elav^{3A}-Gal4* to *UAS-Actin-GFP* or *UAS-Synaptotagmin-GFP* are referred to as controls, whereas larvae from *elav^{3A}-Gal4::UAS-NSF2$^{E/Q}$* crossed to *UAS-Actin-GFP* or *UAS-Synaptotagmin-GFP* are referred to as mutants.

For *NSF2* loss-of-function studies we first made a recombinant chromosome bearing *elav^{3A}-Gal4::Df(3R)urd/TM3, P{w[+mC] = ActGFP}JMR2, Ser^{1}*; the deficiency removes the NSF2 coding region. Second we constructed flies carrying *UAS-Actin-GFP* on the second chromosome and *NSF2^{55}/TM3, P{w[+mC] = GAL4-twi.G}2.3, P{UAS-2xEGFP}AH2.3, Sb^{1} Ser^{1}*. *NSF2^{55}* is a severe loss-of-function allele with a stop codon in the N-terminal domain of NSF2 at amino acid 130 (Golby *et al.*, 2001). Crossing these two lines together, and selecting against the GFP balancer chromosomes, yields offspring that carry *UAS-Actin-GFP; NSF2^{55}/elav^{3A}-Gal4:Df(3R)urd.*

Live and Fixed Larval Preparations and Drug Administration

Wandering third instar larvae were dissected in HL3 physiological saline without calcium (Stewart *et al.*, 1994), and all experiments were conducted in this saline. To minimize movements during image acquisition for fluorescence recovery after photobleaching (FRAP) experiments, the preparation was transferred to a drop of saline on a 3 × 4-inch Sylgard-coated glass slide, stretched out so that the surface of the body wall musculature was flat and immobilized using Nexaband tissue glue (WPI, Sarasota, FL). For fixed preparations, dissected larvae were covered with 4% EM-grade formaldehyde in phosphate-buffered saline (PBS) for 10 min and washed briefly in PBS.

For *NSF2* loss-of-function analysis, first instar larvae were dissected as above with sharpened tungsten wire needles. They were fixed with 4% EM-grade formaldehyde in PBS for 10 min, washed briefly in PBS plus 0.1% Triton X-100 (PBT), incubated in antibody solution as indicated below, washed in PBT, and mounted in Vectashield (Vector Laboratories, Burlington, Ontario, Canada). Four *UAS-Actin-GFP; NSF2^{55}/elav^{3A}-Gal4::Df(3R)urd* and four *UAS-Actin-GFP; NSF2^{55}/elav^{3A}-Gal4* first instar larvae were dissected on the same slide and processed simultaneously under identical conditions. This procedure was carried out twice, and the images shown in Figure 5 are representative of these two genotypes.

The primary antibodies used in this study were rabbit anti-GFP (1:1000, Invitrogen, Burlington, Ontario, Canada), rabbit anti-synaptotagmin (1:2000, gift of N. Reist) and Texas-red–conjugated goat anti-HRP (1:1000; ICN Biomedical, Irvine, CA). The secondary antibodies were goat anti-rabbit Alexa488 and goat anti-rabbit Alexa546 (1:1000, Invitrogen). Rhodamine-phalloidin (Sigma, Oakville, Ontario, Canada) was used at a dilution of 1:1500 in PBT.

Latrunculin A (Sigma) and jasplakinolide (Molecular Probes) were prepared as a 1 mM stock solution in DMSO, and swinholide A (Sigma) was prepared as a 1 mM stock in 100% ethanol. All stock solutions were kept at −20°C, and they were diluted in HL3 to make working solutions at the concentrations indicated in the text. We bath-applied these drugs by exchanging the HL3 solution for HL3 plus the drug; we let the drug incubate for 5 min before image collection and completed image acquisition within 60 min. The preparation was maintained in the drug containing solution throughout the experiment.

Imaging and FRAP

Images in this study were taken from the muscle 6/7 neuromuscular junction in abdominal segments 3 or 4 of wandering third instar larvae.

Live time-lapse images of actin-GFP signals were acquired using a 60× water immersion lens on a Nikon E600FN microscope (Mississauga, Ontario, Canada) equipped with filters appropriate for GFP excitation and emission. Images were acquired with a Hammamatsu ORCA ER camera (Bridgewater, NJ) operated with SimplePCI software (Compix, Sewickley, PA). An Uniblitz shutter (Vincent and Associates, Rochester, NY) was used to minimize the preparation's exposure to fluorescent light; images were acquired once every 15 s with ~1-s exposure time per image. Still images were transformed into movies using SimplePCI (Compix) and digitally stabilized according to the methods described in Fleet and Weiss (2005).

Images of antibody- and phalloidin-labeled nerve terminals were acquired on a LSM510 (Carl Zeiss, Toronto, Ontario, Canada) confocal laser microscope using a 63×/NA 1.4 oil immersion lens. The pinhole on the microscope was set to acquire to images with a focal depth of 1.0 μm. The confocal gain and laser power were identical for both genotypes.

For FRAP analysis, an LSM510 (Carl Zeiss) confocal laser microscope equipped with a 100×/NA 1.0 Achroplan water immersion objective and a 200 mW Argon laser was used. The 488-nm line of the argon laser was set at 3–5% for GFP excitation, and emission was collected though a 505-nm longpass filter. For Syt-GFP images 512 × 512-pixel frames were captured at zooms 8, 9, and 10 (0.02 μm/pixel) with a pinhole setting of 2.0 Airy units (2.4-μm optical sections). The scan speed was set at 6 (6.40 μs/pixel) for higher-quality images and at 12 (0.80 μs/pixel) for faster acquisition. Actin-GFP images were 256 × 256-pixel frames captured a zoom 5 or 6, and the scan speed was 10 (1.76 μs/pixel). Photobleaching was achieved by scanning a 12 × 30-pixel region of interest (ROI) 10 times at 100% laser power. A single frame was captured before the bleaching scan, and 59 frames were acquired every 1.0 s subsequently for Syt-GFP and once every 500 ms for actin-GFP.

For quantifying recovery values we used a recovery index (RI) was defined as follows:

$$RI = (F_p - F_b)/(F_i - F_b) \times 100\%$$

where F_i, F_b, and F_p represent the initial fluorescence, bleached fluorescence, and plateau fluorescence values within the ROI, respectively. This ratio accounts for the differing fluorescence intensities encountered both before and after bleaching among various boutons and preparations. For soluble-GFP and actin-GFP, we normalized the plateau value to the initial value (% recovery); because these two species move rapidly, there is some uncertainty about the lowest bleach level and therefore F_b cannot be measured as accurately.

F-actin Fractionation

Brains from 10 wandering third instar larva were dissected in HL3 solution and incubated in 100 μl HL3 with or without 5 μM swinholide A for 20 min at room temperature. Tissue was then transferred into 100 μl of actin stabilization buffer (Cytoskeleton Inc., Denver, CO; 50 mM PIPES, pH 6.9, 50 mM NaCl, 5 mM $MgCl_2$, 5 mM EGTA, 5% glycerol, 0.1% Nonidet P40, 0.1% Triton X-100, 0.1% Tween 20, 0.1% β-mercaptoethanol, 1 mM ATP, and 1 tablet/50 ml complete protease inhibitor [Roche]) and homogenized with 10 strokes of a glass microtissue grinder. After a 10-min room temperature incubation, samples were spun at 1,000 × *g* for 2 min to remove large debris, and the resulting supernatants were then spun at 100,000 × *g* for 1 h at 22°C in a Beckman optima XL-100K ultracentrifuge with Sw55-Ti rotor and adaptors. Supernatants were carefully removed and pellets were resuspended in SDS sample buffer. Aliquots of samples before ultracentrifugation and the supernatants and pellet after ultracentrifugation were boiled and then separated on 10% SDS-polyacrylamide gels and transferred to PVDF membrane. Actin was detected with mAb JLA20 used at 1:50 dilution (Developmental Studies Hybridoma Bank, University of Iowa, Iowa City, IA) and an HRP-coupled secondary (Bio-Rad, Mississauga, Ontario, Canada) followed by chemiluminescent detection (ECL Plus, Amersham, Baie d'Urfe, Quebec, Canada). Blots were scanned and digitized with a Molecular Dynamics Phosphoimager (Sunnyvale, CA). Band intensities were compared with known amounts of nonmuscle actin (Cytoskeleton Inc.) run on the same gel and quantified using ImageJ (NIH).

Data Analysis

All images were analyzed using the Zeiss LSM-510 software or the open-source application ImageJ 1.32j. All statistical tests and curve fitting were performed using Prism 4.0 (GraphPad Software, San Diego, CA) using tests indicated in the text. We chose $p < 0.05$ as the level of statistical significance, and unless otherwise indicated, data are presented as mean ± SEM throughout the text. Figures were assembled using the open-source application Inkscape.

RESULTS

Reduced Synaptic Vesicle Mobility in NSF2$^{E/Q}$ *Boutons*

To test the hypothesis that the *NSF2$^{E/Q}$* has altered synaptic vesicle mobility, we applied FRAP analysis to control and *NSF2$^{E/Q}$* larval NMJs. We used a synaptotagmin-GFP (Syt-GFP) fusion protein to label synaptic vesicles and photobleached small regions of single synaptic boutons and then measured the movement of the GFP signal back into the bleached area (Figure 1).

In controls, we observed recovery of the fluorescent signal such that within one minute the signal had returned to ~80% of its original value. In contrast, when identical pro-

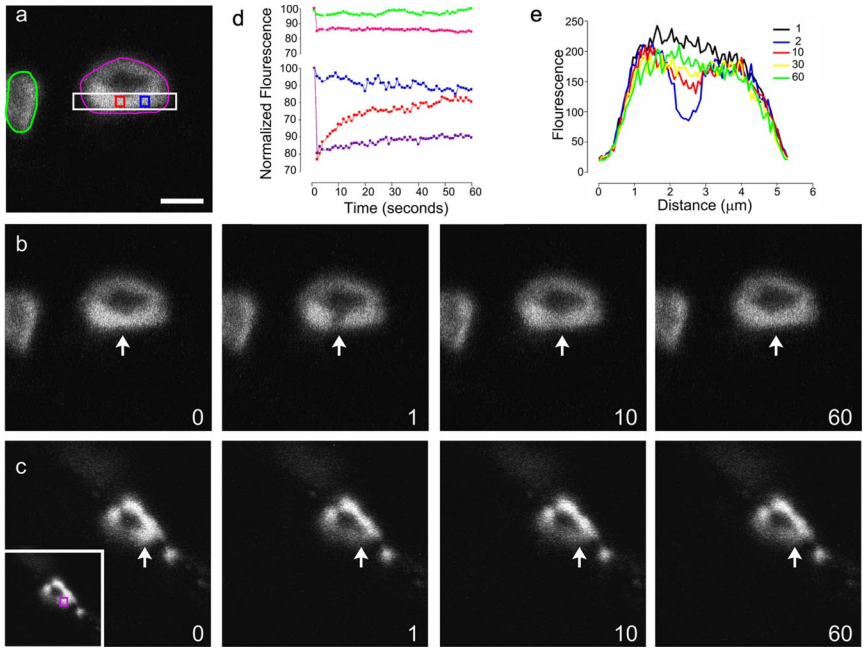

Figure 1. FRAP analysis of synaptic vesicle mobility. (a) An image of Syt-GFP within the nerve terminal boutons of a control (*elav^{3A}-Gal4 × UAS-SytGFP) Drosophila* larva. Colored shapes indicated the regions from which mean fluorescence intensities were taken and are shown in subsequent panels. (b) Time sequence of the same bouton before (0), immediately after photobleaching (1), 10 s (10), and 60 s (60) after bleaching. The arrow indicates the 12 × 30-pixel region that was bleached. (c) SytGFP expression in a mutant (*elav^{3A}-Gal4::UAS-NSF2$^{E/Q}$ × UAS-SytGFP*) larva shown at the same time intervals as in panel b; the arrow indicates the region that was photobleached. The inset shows the area (purple square) from which mean fluorescence intensity was measured. (d) The time course of changes in fluorescence intensity for the colored regions indicated in panels a and c. The red line represents the region within the bleach zone, and the blue line a region adjacent to the bleach zone; the pink line is the average intensity of the whole target bouton, and the green line is the average intensity of a neighboring bouton. The purple line represents the bleached region in the mutant bouton shown in c. (e) Each colored line represents the mean fluorescence intensity from the cross-section indicated by the white rectangle in panel a, at times 0, 1, 10, 30, and 60 s. Scale bar, (a) 2.5 μm.

cedures were applied to *NSF2$^{E/Q}$* boutons the recovery was much reduced and in some cases there was little or no recovery observed (Figure 2). To compare the responses between the genotypes we used a recovery index that accounts for both initial fluorescence intensity and the amount of bleaching (see *Materials and Methods*). We found that, on average, there was about half as much recovery observed in the *NSF2$^{E/Q}$* compared with the control genotype (Figure 2). The recovery index for the control samples was 58.5 ± 1.5 (arbitrary unit ± SEM, n = 63 boutons from 9 larvae), whereas for the mutant samples it was 32.5 ± 2.1 (n = 49 boutons from 6 larvae).

We carried out several control experiments to ensure this was the correct result. First, to be certain that the recovery was due to organelle movement and not spurious recovery of fluorophore activity, we fixed the Syt-GFP expressing larvae in 4% formaldehyde before FRAP analysis, and we observed no fluorescence recovery in the bleached area (5 boutons, 2 larvae). Second, for positive controls we applied FRAP to soluble GFP and plasma-membrane–bound GFP (mCD8-GFP) in both *NSF2$^{E/Q}$* and control genetic backgrounds, and we observed equally robust recovery for both of these signals. The sample sizes for these groups were: control CD8-GFP, 22 boutons from 2 larvae; *NSF2$^{E/Q}$* CD8-GFP, 27 boutons from 2 larvae; control soluble-GFP, 19 boutons from 2 larvae; and *NSF2$^{E/Q}$* soluble-GFP, 10 boutons from 3 larvae. The above data were subjected to ANOVA, and significant variance was found between the groups ($p < 0.0001$). Post-test comparisons of the two genotypes, revealed that there is significant difference between the control and mutant for Syt-GFP samples ($p < 0.001$), but no significant difference between the genotypes in the soluble GFP or the mCD8-GFP samples. Thus, these data show that our measurement of fluorescence recovery in the bleached zones genuinely represents synaptic vesicle mobility and that mobility is reduced in the *NSF2$^{E/Q}$* larvae.

Fitting the FRAP recovery curve with a one-phase exponential equation (Figure 2) yielded a time constant for recovery of 3.5 ± 0.2 s in the control samples, whereas it was 6.3 ± 0.4 s in the mutant samples. The difference between the genotypes is significant (*F* test, $p < 0.001$). This indicates that the vesicles in the control nerve terminal move at a faster rate than those moving within the mutant nerve terminal. Thus, our FRAP analysis of vesicle mobility shows that the *NSF2$^{E/Q}$* transgene substantially impairs both the extent and the rate of vesicle movement within individual presynaptic boutons.

Swinholide Impairs Vesicle Mobility in Control Terminals, Whereas Latrunculin Restores Vesicle Mobility in NSF2$^{E/Q}$ *Terminals*

To determine if there is a relationship between vesicle mobility and presynaptic actin, in a separate set of trials we applied the F-actin severing drug swinholide A, the F-actin–depolymerizing drug latrunculin A, and the F-actin–stabilizing drug jasplakinolide (Bubb *et al.*, 1995; Spector *et al.*, 1999) to control and *NSF2$^{E/Q}$* nerve terminals. First, swinholide (Figure 3a) and latrunculin (unpublished data) both lead to redistribution of actin-GFP within a few minutes (see also *NonUniform Distribution of Actin* below), whereas there was no change in Syt-GFP distribution upon application of the drug, or up to 40 min afterward. When we measured the FRAP recovery index for nontreated control preparations, we found a mean value of 62.6 ± 2.1 (n = 20 from 5 larvae) and for control preparations treated with 5 μM swinholide a value of 49.3 ± 2.5 (n = 41 from 3 larvae), and for control preparations treated with 10 μM latrunculin a value of 54.8 ± 2.2 (n = 43 from 7 larvae) was found. The value for *NSF2$^{E/Q}$* nontreated nerve terminals was 24.8 ± 1.7 (n = 58 from 10 larvae) and for *NSF2$^{E/Q}$* swinholide- and latrunculin-treated terminals the respective values were 30.7 ± 2.9 (n = 23 from 3 larvae) and 46.6 ± 2.4 (n = 36 from 4 larvae). After application of 10 μM jasplakinolide, the FRAP recovery index was 61.6 ± 1.3 (n = 27 from 2 larvae) in the controls and 32.7 ± 1.3 (n = 23 from 2 larvae) in *NSF2$^{E/Q}$* boutons.

A two-factor ANOVA (genotype X drug) showed that there was a significant effect of the genotype ($F_{1,263} = 199.7$,

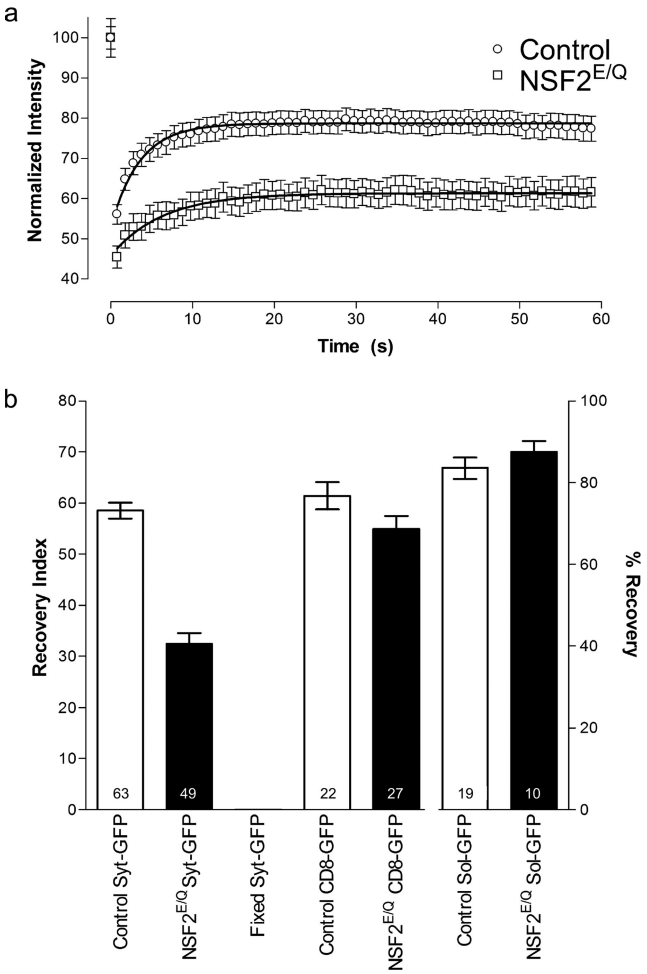

Figure 2. Summary of FRAP analysis. (a) The time course of fluorescence intensity changes. The symbols represent the mean value from each of control and *NSF2*$^{E/Q}$ boutons at each time point. Error bars, SEM. Lines are best fit to the one-phase exponential equation $y = A(1 - e^{(-k/x)}) + B$. (b) Summary of recovery index values, where the bars represent the mean value and the error bars the SEM for each of the genotypes and conditions indicated. The right axis, % recovery, applies only to the pair of sol-GFP bars. Sample size: n = number of boutons is indicated on each bar; the number of larvae were control, 9; *NSF2*$^{E/Q}$, 6; fixed, 2; control CD8-GFP, 2; *NSF2*$^{E/Q}$ CD8-GFP, 2; control sol-GFP, 2; and *NSF2*$^{E/Q}$ sol-GFP, 2.

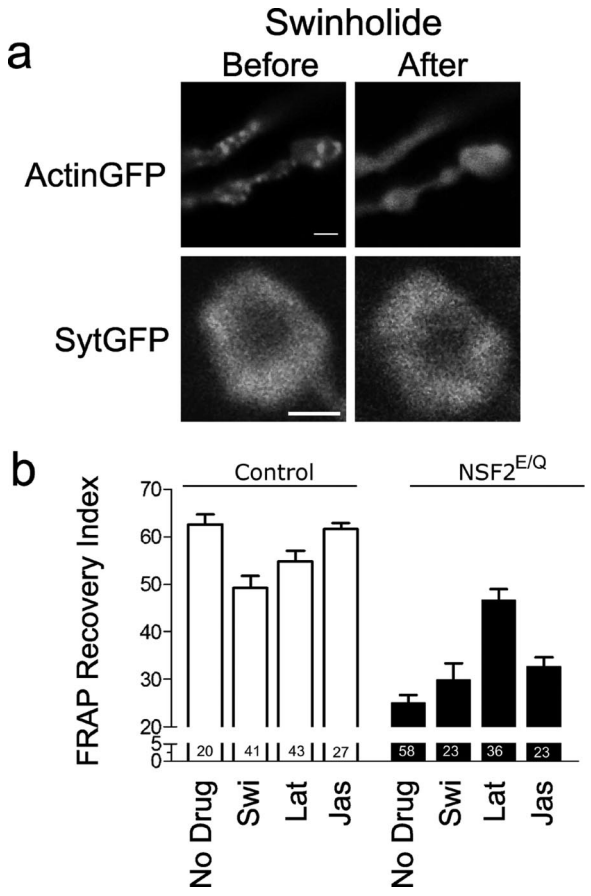

Figure 3. Effect of swinholide and latrunculin on vesicle mobility. (a) Images of actin-GFP and Syt-GFP before and after application of 5 μM swinholide. The normally punctate distribution of actin is abolished after drug treatment (the scale bar for actin-GFP image is 2 μm), whereas the donut-shaped synaptotagmin signal remains virtually unchanged. This image was taken 40 min after application of swinholide (scale bar for Syt-GFP image is 1.5 μm) (b) Summary of recovery index values in the absence of drug or in the presence of 5 μM swinholide (Swi), 10 μM latrunculin (Lat), or 10 μM jasplakinolide (Jas), where the bars represent the mean value and the error bars the SEM for each of the genotypes and conditions indicated. Sample size (n = number of boutons) is indicated on each bar; the number of larvae were as follows: control no drug, 5; control + Swi, 3; control + Lat, 7; control + Jas, 2; *NSF2*$^{E/Q}$, 5; *NSF2*$^{E/Q}$ + Swi, 3; *NSF2*$^{E/Q}$ + Lat, 4; and *NSF2*$^{E/Q}$ + Jas, 2.

$p < 0.001$), a significant effect of the drugs ($F_{3,263} = 7.4$, $p < 0.001$), and a significant interaction ($F_{3,263} = 14.7$, $p < 0.001$). A Bonferroni post-test of the no drug versus drug treatments within each genotype revealed a significant difference between the swinholide-treated and nontreated boutons in the control group ($p < 0.01$) but not the *NSF2*$^{E/Q}$ group. For latrunculin treatment, the difference between no drug and latrunculin-treated control groups was smaller, though the effect was significant ($p < 0.05$). Surprisingly, latrunculin-treated *NSF2*$^{E/Q}$ boutons showed a significant increase in the recovery index compared with nontreated *NSF2*$^{E/Q}$ boutons ($p < 0.01$). Finally, there was no effect of jasplakinolide on the control response, whereas there was a modest increase in recovery in the mutants ($p < 0.05$).

Distribution of Actin in the Nerve Terminal

To assess the distribution of actin within the nerve terminal we expressed an *UAS-Actin-GFP* transgene in neurons of the control and *NSF2*$^{E/Q}$ genotypes. We could easily identify GFP fluorescence within the CNS and in the presynaptic nerve terminal. Interestingly, the GFP signal within control synaptic boutons was not uniform, but rather very punctate in appearance (Figure 4a). In contrast, actin-GFP distribution in the *NSF2*$^{E/Q}$ boutons was predominantly uniform with many fewer punctate concentrations of GFP found throughout the nerve terminal. These data indicate there is a substantial alteration in actin distribution within the mutant nerve terminals.

We examined this prominent phenotype in an *NSF2* loss-of-function allele to verify the effect on actin. We first established fly stocks carrying the severe *NSF2*^{55} allele and the *UAS-Actin-GFP* transgene and crossed these to a stock with a recombinant chromosome bearing *elav*^{3A}*-Gal4* and *Df(3R)urd*, a deletion that removes the *NSF2* gene. We then selected *NSF2*^{55}/*Df(3R)urd* first instar larvae for dissection and examined actin-GFP at the nerve terminal. Control larvae for this experiment

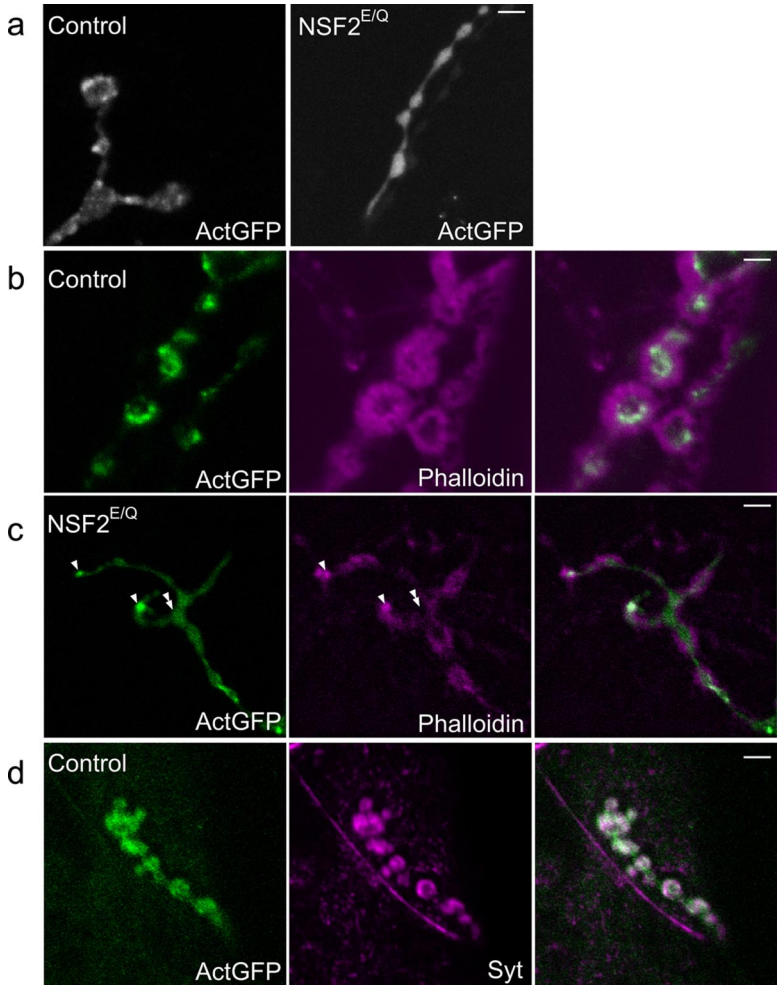

Figure 4. Altered actin distribution and localization of F-actin in *NSF2*$^{E/Q}$ boutons. (a) Images are of actin-GFP distribution in control and *NSF2*$^{E/Q}$ nerve terminals. In controls the GFP signal shows a nonuniform punctate appearance, whereas in the *NSF2*$^{E/Q}$ nerve terminal it is much more diffuse. (b) Single-slice confocal images of control actin-GFP–expressing nerve terminal labeled with phalloidin reveals that the actin-GFP puncta correspond to filamentous actin. Most of the phalloidin signal in this image is postsynaptic, corresponding to the subsynaptic reticulum of the muscle; however, the presynaptically expressed GFP coincides with phalloidin labeling. (c) Similar image of actin-GFP expressing *NSF2*$^{E/Q}$ boutons. This image was selected because it shows the exclusion of phalloidin signal from the actin-GFP signal, marked by the double arrowhead, whereas there are some GFP concentrations that do coincide with phalloidin, marked by the single arrowheads. (d) Colocalization of actin-GFP with synaptotagmin. Control nerve terminals expressing actin-GFP were immunostained with an antibody against *Drosophila* synaptotagmin. The two signals overlap to a great extent, but there are some areas in which the GFP signal is seen in the absence of Syt labeling. Scale bars, 4 μm.

were *UAS-Actin-GFP; elav*^{3A}*-Gal4:Df(3R)urd/+*. GFP fluorescence levels were low in the NMJ at this stage so we fixed and processed the tissue for anti-GFP antibody labeling. In the control samples, we could see punctate distribution of actin-GFP within nerve terminal boutons. In the *NSF2*^{55}*/Df(3R)urd* NMJs1, however, we did not observe such a distribution; rather, the signal was uniform throughout the boutons, similar to our observations on the *NSF2*$^{E/Q}$ allele at the third instar stage. Figure 5a shows example NMJs at low magnification, whereas Figure 5b shows higher magnification images in which the tissue is double-labeled with anti-HRP, as a general nerve terminal marker. These data therefore indicate that there is a redistribution of presynaptic actin in both *NSF2* loss-of-function and dominant negative alleles.

To understand the polymerization state of actin within the nerve terminals, we fixed and labeled both control and *NSF2*$^{E/Q}$ third instar larvae expressing actin-GFP with rhodamine-phalloidin (Rh-Ph), a compound that binds exclusively to F-actin. In these preparations Rh-Ph labels the contractile actin, which is below the plane of focus in Figure 4, b and c, as well as F-actin in the subsynaptic reticulum surrounding the boutons. This limits our ability to differentiate pre- and post-synaptic F-actin. However, because the actin-GFP puncta are relatively large and are presynaptic because of the neural expression of the transgene, we took single-plane 1-μm confocal images through the center of boutons and addressed the Rh-Ph localization. We found that in the control preparations the presynaptic actin-GFP puncta coincide with Rh-Ph labeling, indicating these bright spots most likely correspond to F-actin (Figure 4b). In the *NSF2*$^{E/Q}$ nerve terminal we found two patterns (Figure 4c). First, the predominant pattern was that the nonpunctate actin-GFP did not colocalize with Rh-Ph labeling; rather the two signals appeared to be exclusive. Second, where we did observe a few actin-GFP puncta in the *NSF2*$^{E/Q}$, we did see colocalization. These data therefore suggest that there is a reduction in the amount of F-actin within the *NSF2*$^{E/Q}$ nerve terminal.

In control preparations we also examined the distribution of actin-GFP relative to synaptic vesicles using an antibody against the synaptic vesicle protein, synaptotagmin. Our results showed that the two signals colocalize to a great extent (Figure 4d). This result is in accord with the knowledge that synaptic vesicles occupy a large volume within *Drosophila* nerve terminal boutons, and they often occupy an outer ring of the synaptic bouton with an empty center. The actin-GFP concentrations also appear primarily in an outer ring. These data place actin in the correct subcellular location to influence synaptic vesicle movement.

Rapid Movement of Actin within the Nerve Terminal

To expand our examination of actin within presynaptic boutons, we made time-lapse movies of the actin-GFP signals from live larval NMJs. We surprisingly observed that the punctate structures seen in the fixed preparation were not stable but rather constantly moving in living preparations

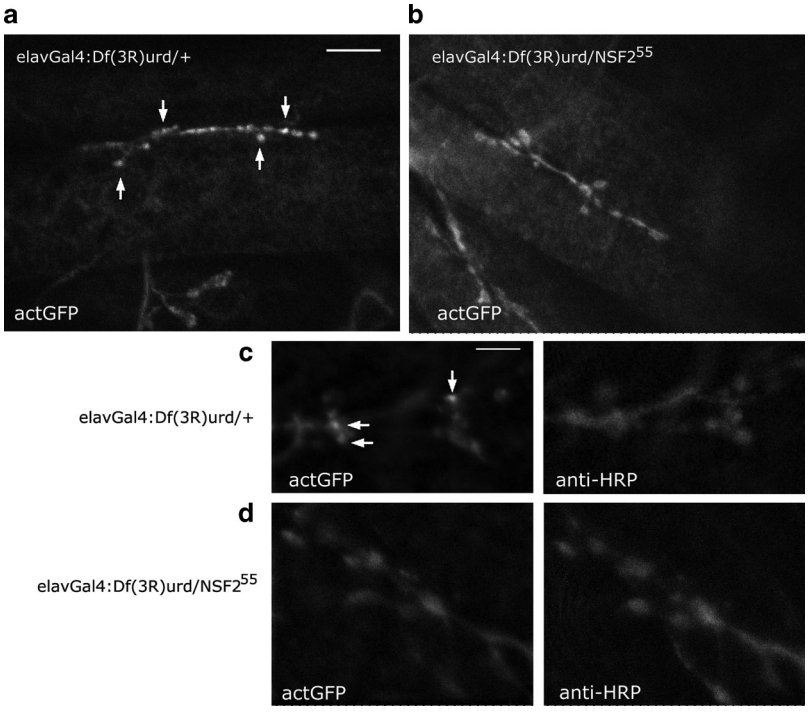

Figure 5. Altered actin distribution in an *NSF2* loss-of-function allele. (a and b) First instar larval NMJs from *Df(3R)urd/+* and *Df(3R)urd/NSF2^{55}* expressing actin-GFP. Clear concentrations of the actin-GFP signal can be seen in the controls (arrows), but these are absent in the loss-of-function allele. Images were acquired at the same confocal settings. Scale bar, 10 μm. (c and d) A second pair of NMJs shown at higher magnification and double-labeled with the neural marker anti-HRP. Clear actin-GFP puncta are visible (arrows) within the *Df(3R)urd/+* NMJs, whereas in the *Df(3R)urd/NSF2^{55}* boutons the actin-GFP appears diffuse and the puncta are not apparent.

(Figure 6; Supplementary Videos 1 and 2). In contrast, actin-GFP dynamics seemed reduced in the *NSF2$^{E/Q}$* terminals (Supplementary Videos 3 and 4).

To begin our analysis of these data, the time-series images were first stabilized and segmented to select the pixels that represent the nerve terminal. There was about a 10% decrement in fluorescence intensity through the time series due to photobleaching, and therefore individual pixel intensities were linearly adjusted for changes in the overall mean intensity of all the pixels. The fluorescence intensity values for each pixel were placed into a three-dimensional matrix (x and y coordinates and time), and the mean and SD for each pixel through the time series was calculated. We reasoned that the variation of pixel intensity over time for each individual pixel should be greater for samples in which GFP is moving rapidly than for samples in which there is reduced movement. Accordingly, the frequency distribution of the SDs for each analyzed pixel, from five control and five *NSF2$^{E/Q}$* NMJs, is shown in Figure 6b. It can be seen that the control cells uniformly have a higher proportion of pixels with large SDs, in comparison to the mutant cells, which have a greater proportion of pixels with small SDs. The mean of the SD ($\pm$95% confidence interval) was 5.61 $\pm$ 0.07 from controls and 4.03 $\pm$ 0.08 from mutants. Thus we conclude that there is a significant reduction in presynaptic actin dynamics in the *NSF2$^{E/Q}$* nerve terminal.

We further we utilized this technique to examine the effects of swinholide, latrunculin, and jasplakinolide. Time-lapse imaging of NMJs treated with jasplakinolide showed that all GFP movement ceased upon application (unpublished data), whereas NMJs treated with the other two drugs show dispersion of the actin-GFP puncta. We quantitated four jasplakinolide-treated images series and five each for latrunculin and swinholide; the results are shown in Figure 6b. As expected, the individual pixel data show that the drug-treated samples have markedly less variation in fluorescence intensity over time, and thus nearly all of the pixels have small SDs. The mean of the SDs ($\pm$95% confidence interval) was 3.2 $\pm$ 0.02 for the jasplakinolide-treated samples, 2.1 $\pm$ 0.03 for the swinholide-treated sample, and 2.0 $\pm$ 0.01 for latrunculin-treated sample. ANOVA of the control, mutant, and control plus drug-treated cells revealed significant variation among them ($p < 0.0001$), and post-tests showed each group to be different from each other ($p < 0.001$ for each comparison).

To examine the possibility that the observations we made on actin-GFP were inadvertently due to the overexpression of actin within the nerve terminal, we used a moesin-GFP transgene as a reporter of actin at the synapse. This transgene contains only the actin-binding domain of moesin, fused to GFP, and it has been used in prior studies as a reporter of actin in living tissue (Edwards *et al.*, 1997). Just as we saw with the actin-GFP, the moesin-GFP reporter shows a punctate nonuniform distribution within synaptic boutons, and time-lapse imaging of moesin-GFP also shows rapid movement within the boutons (unpublished data). This result substantiates the fact that actin-GFP is being incorporated into the normal actin biochemical pathway and that our observations with actin-GFP are not an artifact due to overexpression of actin.

Fractionation of Actin

To complement the above findings, we measured the relative amounts of filamentous actin in the *NSF2$^{E/Q}$* and control neurons with a biochemical approach. Using larval brain homogenates as our starting material, we utilized high-speed centrifugation to separate filamentous and monomeric actin, followed by SDS-PAGE and Western blotting. We analyzed five independently prepared samples; in three of these we used the *yw* strain as the control genotype, whereas in the other two we used *elavGal4× UAS-NSF2^{WT}* as the control. In each of the five trials there was an equal amount of actin found in the input homogenates in both the control and *NSF2$^{E/Q}$* genotypes but there was less actin in the high-speed pellet prepared from *NSF2$^{E/Q}$* samples than in controls (Figure 7). From three paired trials, there was 27,

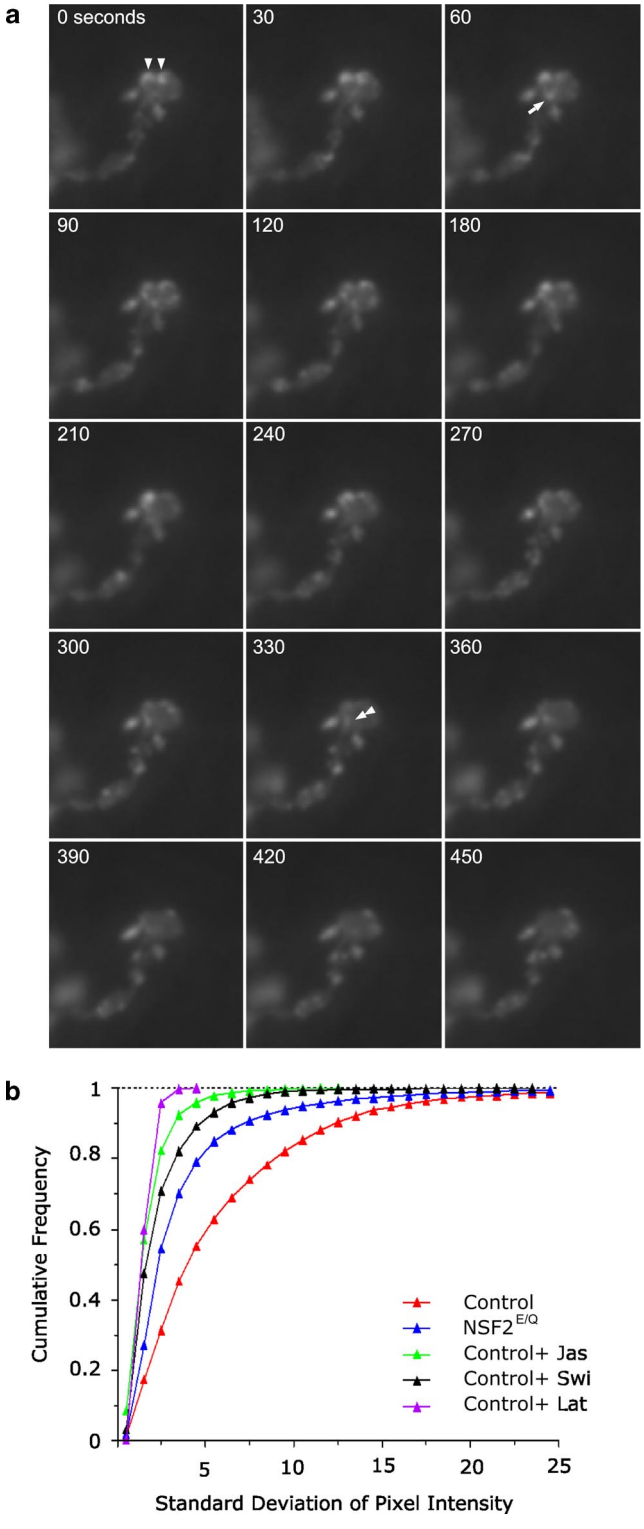

Figure 6. Presynaptic actin is dynamic. (a) Time-lapse image sequence of actin-GFP expressed in a control nerve terminal. The time elapsed from the beginning of the sequence is indicated in the top left corner. The punctate actin structures indicated by the triangles at time zero have moved laterally by the end of the series, whereas the puncta indicated by the arrow at time 60 increases in brightness and then disappears by time 240. Finally, at time 330 some actin-GFP, at the double triangle, appears to splinter off a larger puncta and move down and out of the bouton. (b) A frequency distribution of the SD of individual pixels over the time series of image acquisition. The control (*elav^{3A}-Gal4* × *Actin-GFP*) genotype has a greater proportion of pixels with high SD in comparison to the mutant (*elav^{3A}-Gal4::UAS-NSF2$^{E/Q}$*× *UAS-Actin-GFP*) genotype or the control genotype treated with jasplakinolide, swinholide, or latrunculin. These data were compiled from time-lapse image series of 5 NMJs from 4 control larvae, 5 NMJs from 4 mutant larvae, and 4 NMJs from 3 larvae for each of the control plus drug treatment.

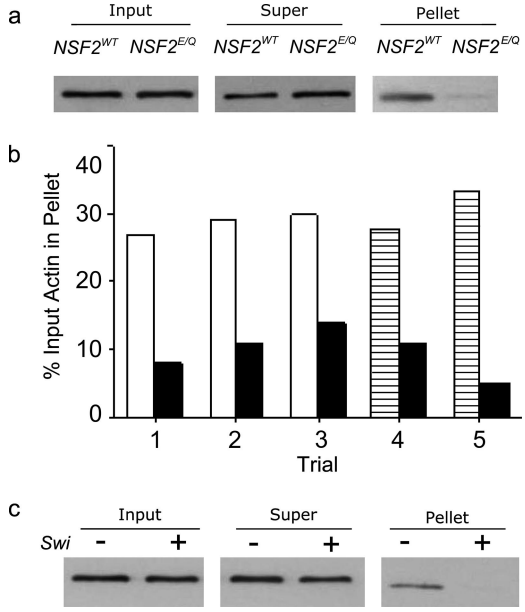

Figure 7. Actin Fractionation. (a) Larval brain homogenates were examined for actin before and after high-speed centrifugation by SDS-PAGE and Western blotting. This image is an example Western blot showing the input and the supernatant and pellet fractions. The input homogenates from *elav-Gal4* × *NSF2^{WT}* and *elav-Gal4* × *NSF2$^{E/Q}$* samples were equivalent but the amount of actin found in the pellet appears less for the *NSF2$^{E/Q}$* sample. (b) Quantification of the amount of actin in high-speed pellet, expressed as a percentage of the input actin, for each of five trials. In all trials, the black bars represent the *elav-Gal4* × *NSF2$^{E/Q}$* result. For trials 1, 2, and 3 the open bars represent data obtained from *yw* controls, whereas for trials 4 and 5 the hatched bars represent data from *elav-Gal4* × *UAS-NSF2^{WT}* controls. (c) Pretreatment of larval brain homogenates eliminates actin detected in the pellet fraction. Twenty brains were dissected from *elav-Gal4* × *UAS-NSF2^{WT}* larvae, 10 were incubated in HL3 alone, and 10 were incubated in HL3 plus 5 μM swinholide followed by centrifugation, SDS-PAGE, and Western blotting. There was no detectable signal in the pellet samples that were pretreated with swinholide, indicating the signal in untreated samples arises from F-actin. This blot is representative of two independent trials with swinholide pretreatment.

29, and 30% of total actin in the *yw* pellet compared with 8, 11, and 14% in the *NSF2$^{E/Q}$* strain. In the *elav-Gal4*× *UAS-NSF2^{WT}* strain there was 27.5 and 33% of the actin was in the pellet compared with 11 and 5% for the *NSF2$^{E/Q}$* strain (Figure 7b). Therefore, on average we found two thirds less actin in the pellet from the mutant samples. To be certain that the signal observed in the pellet fraction genuinely represents actin filaments, we pretreated the larval brains with 5 μM swinholide A and found that there was no longer actin in the high-speed pellet (Figure 7c). Therefore, this fractionation data indicates that there is less F-actin in the *NSF2$^{E/Q}$* brain and corresponds to our imaging data at the NMJ.

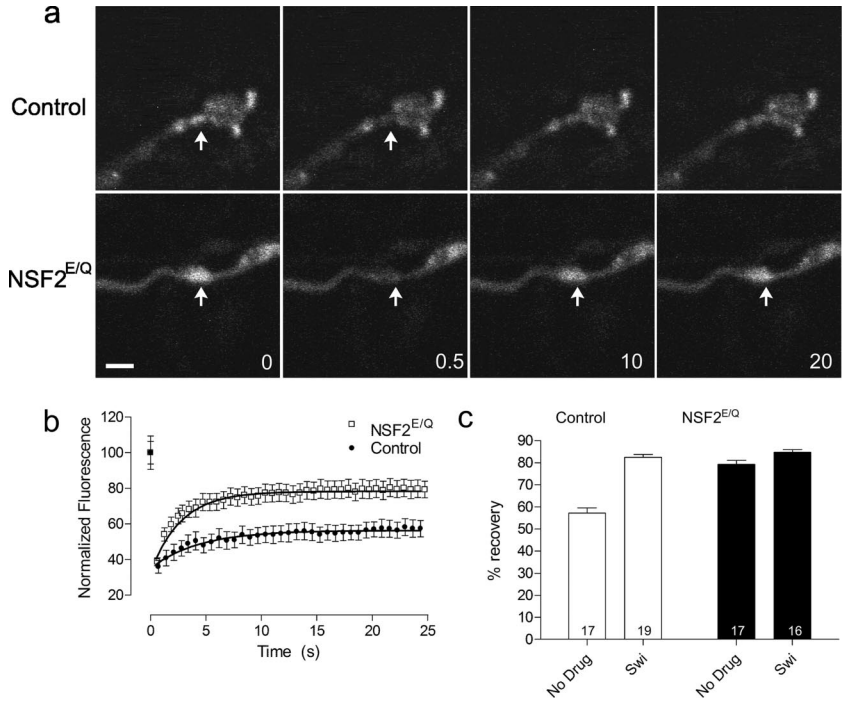

Figure 8. Frap analysis of actin-GFP. (a) Images of control (*elav*^{3A}*-Gal4* × *Actin-GFP*) and *NSF2*$^{E/Q}$ (*elav*^{3A}*-Gal4::UAS-NSF2*$^{E/Q}$ × *UAS-Actin-GFP*) nerve terminals expressing actin-GFP subjected to FRAP. Arrow indicates the region that was photobleached, 0 indicates before photobleaching, 0.5 is immediately after photobleaching, and 10 and 20 are 10 and 20 s after photobleaching. Scale bar, 5 μm. (b) The time course of recovery of actin-GFP signal after photobleaching, where the symbols represent the mean value and the bars the SEM at each time point. The line is the best fit of the one-phase exponential equation $y = A(1 - e^{(-k/x)}) + B$ to the recovery data points. Scale bar, 2 μm. (c) Summary of the % recovery values obtained for control and *NSF2*$^{E/Q}$ boutons, in the absence or presence of 5 μM swinholide. Sample size (n = number of boutons) is indicated on each bar, from three larvae each.

FRAP Analysis of Actin Mobility

Lastly, to better determine the relative abundance of F- and G-actin within the nerve terminal, we used FRAP analysis of actin-GFP. Boutons with a higher proportion of G-actin should show greater recovery after photobleaching because the small monomeric molecule should have greater mobility than the larger polymerized F-actin.

Before examining live preparations we first established our FRAP parameters on actin-GFP synaptic boutons that were fixed in 3.7% formaldehyde. We found we could bleach a small section of the synaptic bouton using our microscope with 15 scans of a small region of interest at 100% laser power. In the fixed preparations fluorescence did not reappear in the bleached area, indicating there is no spontaneous recovery of GFP fluorescence.

We next applied FRAP analysis to live preparations of control and *NSF2*$^{E/Q}$ larvae that were untreated or treated with 5 μM swinholide (Figure 8). In the untreated control boutons we observed that the fluorescence intensity returned to 57.9 ± 2.5% (n = 17 from 3 larvae) of its original value. In contrast, untreated *NSF2*$^{E/Q}$ boutons showed substantially more recovery, returning to 77.8 ± 1.5% (n = 17 from 3 larvae). This result suggests that there is more G-actin actin within the *NSF2*$^{E/Q}$ boutons than in controls. This idea is substantiated by our finding that recovery increases to 77.4 ± 5.0% (n = 19 from 3 larvae) after swinholide treatment of control boutons. In mutant boutons, actin mobility is unchanged after swinholide, with the recovery level being 81.9 ± 1.2% (n = 16 from 3 larvae) after treatment.

A two-factor ANOVA (genotype X drug) of the FRAP actin-GFP data showed that there was a significant effect of the genotype ($F_{1,65}$ = 49.87, p <0.001), a significant effect of the drug ($F_{1,65}$ = 79.61, p < 0.001), and a significant interaction ($F_{1,65}$ = 32.8, p < 0.001). A Bonferroni post-test of the revealed a significant difference between the swinholide-treated and nontreated boutons in the control genetic background (p < 0.001) but not no effect in *NSF2*$^{E/Q}$ group. Therefore, from this FRAP experiment we conclude that ~60% of the actin in the control nerve terminal is filamentous, whereas the *NSF2*$^{E/Q}$ nerve terminal has ~25% F-actin.

DISCUSSION

In this article we report that a transgene designed to impair NSF activity leads to a substantial reduction in synaptic vesicle mobility. This impairment is associated with altered distribution and polymerization of presynaptic actin. Application of actin-filament–disrupting drugs decreases synaptic vesicle mobility in control boutons but does not further reduce movement in *NSF2*$^{E/Q}$ boutons. Three independent lines of evidence indicate that there is a reduction in actin filaments within *NSF2*$^{E/Q}$ boutons, and FRAP analysis of actin indicates an increase in the proportion of G-actin. Altogether these data suggest first that F-actin promotes intrabouton vesicle mobility and second that NSF may have a role in establishing or maintaining actin filaments.

Synaptic Vesicles Are Mobile in the Resting Nerve Terminal

Although previous reports have used optical methods to examine synaptic vesicle mobility, our analysis provides new insight into this process. We found a high rate of synaptic vesicle mobility at the unstimulated *Drosophila* larval NMJ, with time constants of recovery measuring ~3–4 s. Our results are most similar to those reported for the ribbon-type synapse of goldfish retinal bipolar cells (Holt *et al.*, 2004), where vesicle recovery times after photobleaching are also less than 1 min, but our results are in contrast to the lack of mobility reported for vesicles at the frog NMJ and hippocampal cultured neurons (Henkel *et al.*, 1996; Kraszewski *et al.*, 1996). The differences may reflect genuine biological differences between types of synapses; the *Drosophila* NMJ is a high-output synapse, whereas hippocampal synapses are not. Also, the dependence on Synapsins is different. While Synapsin mutants of *Drosophila* are viable and have normal neurotransmission at the larval NMJ (Godenschwege *et al.*,

2004), in vertebrates Synapsin is known to link vesicles to actin and to be important for normal synaptic release (Rosahl *et al.*, 1995; Hilfiker *et al.*, 2005).

Some of the inconsistencies between our data and the previous reports may also arise from technical differences. The clearest divergence between our approach and the previous reports is in the vesicle label used. We used a genetically encoded marker for synaptic vesicles, whereas the previous studies have relied on uptake of FM1-43. Because loading of such dyes requires substantial synaptic vesicle exo- and endocytosis, it is not possible to examine synapses that have not been recently activated, whereas we examined vesicle mobility in the resting preparation. A further complication associated with FM1-43 is that it may incorporate into nonvesicle cisternae (Richards *et al.*, 2000), which would present an obstacle to measuring synaptic vesicle mobility. One previous report using a genetically encoded VAMP-GFP construct found low vesicle mobility (Estes *et al.*, 2000), but in that case a very long photobleaching time of 25 s was used. In our hands, photobleaching exceeding 1 s led to substantial photodamage (Nunes and Stewart, unpublished results). It therefore seems likely that photodamage was a contributing factor to the low vesicle mobility of this previous report.

Actin in the Presynaptic Nerve Terminal

To date, the role actin plays in the nerve terminal is unclear, particularly with respect to exocytosis (Doussau and Augustine, 2000). Differing reports ascribe inhibitory (Wang *et al.*, 1996; Bernstein *et al.*, 1998; Morales *et al.*, 2000), positive (Kuromi and Kidokoro, 1998; Cole *et al.*, 2000; Sakaba and Neher, 2003), or supportive (Sankaranarayanan *et al.*, 2003) roles in synaptic vesicle mobilization. The data herein support the idea that actin filaments promote intrabouton mobility of synaptic vesicles. Like Sankaranarayanan *et al.* (2003), we also found no disruption of the synaptic vesicle cluster after application of actin-depolymerizing drugs. However, when we examined movement of vesicles within a bouton, we did find a role for actin. Thus, actin is a cytoskeletal element important for short travel distances within a bouton.

Previous studies have examined the presynaptic distribution of actin at the synapse. At the frog neuromuscular junction (Dunaevsky and Connor, 2000; Richards *et al.*, 2004), and the lamprey reticulospinal synapse (Shupliakov *et al.*, 2002) actin appears excluded from active zones, whereas at synapses of hippocampal cells in culture actin localizes with and surrounds the vesicle cluster (Sankaranarayanan *et al.*, 2003). Our fixed preparations of actin show a high degree of colocalization with synaptic vesicles, most like the hippocampal synapse; this observation is made more important by our finding that actin is very dynamic within presynaptic cytoplasm.

The Nerve Terminal Cytoskeleton Is Dynamic

We were surprised to find the nonuniform distribution of actin-GFP. These concentrations of actin correspond to filamentous actin, and we were further surprised to observe that puncta move dynamically within and between nerve terminal boutons. It seems likely that the images we see represent the rapid polymerization and depolymerization of actin, but the biological function of this activity is not certain. In some respects these observations are similar to those made on mast cell vesicle movement (Merrifield *et al.*, 1999), in that actin comet tails have a role in pushing vesicles away from the plasma membrane toward the interior of the cell. Presently, we do not favor this model for the synaptic vesicle movement we measured here because the actin-stabilizing drug jasplakinolide stops actin-GFP puncta movement but it did not have an effect on our FRAP measurements of vesicle movement.

NSF2$^{E/Q}$ *Disrupts Vesicle Mobility and F-Actin*

We have reported that expression of *NSF2*$^{E/Q}$ in neurons leads to a reduction in the size of the vesicle pool that could be measured physiologically (Stewart *et al.*, 2002). One potential explanation of this phenotype is disruption of endocytosis or generally reduced vesicle delivery to the nerve terminal. Both of these alternatives predict fewer vesicles in the boutons. Indeed, electron microscopic studies of bona fide endocytosis mutants show a clear and obvious reduction in the vesicle population (Zhang *et al.*, 1998; Verstreken *et al.*, 2002, 2003; Koh *et al.*, 2004). However, when we examined the nerve terminal ultrastructure of the *NSF2*$^{E/Q}$ larvae, we found no alteration in the total number of vesicles (Stewart *et al.*, 2005). These data support the notion that there is not a major defect in endocytosis. We therefore proposed that a defect in intrabouton vesicle mobility may be at the heart of the observed phenotype. That possibility was directly tested here, and indeed we found that vesicles in the *NSF2*$^{E/Q}$ nerve terminal are about half as mobile as those in controls.

Because our previous genetic data revealed that coexpression of actin or several actin regulators suppresses the NMJ overgrowth phenotype associated with *NSF2*$^{E/Q}$ expression (Laviolette *et al.*, 2005), we investigated the state of actin within the *NSF2*$^{E/Q}$ nerve terminal. Three of our data sets indicate that there is reduced F-actin at the *NSF2*$^{E/Q}$ nerve terminal. First, we showed that the punctate actin-GFP signal in controls corresponds to F-actin, that these puncta are reduced in the *NSF2*$^{E/Q}$ boutons, and that phalloidin staining is likewise reduced in the *NSF2*$^{E/Q}$ line; second, we used a centrifugation approach to separate F-actin, and we found that there is less F-actin in protein pellets prepared from *NSF2*$^{E/Q}$ brain homogenates compared with controls; and third, we showed an increased mobility of actin-GFP in *NSF2*$^{E/Q}$ boutons by FRAP analysis. We ruled out potential confounding effects of transgene expression by showing the similarity of actin-GFP distribution in a genuine *NSF2* loss-of-function allele compared with that in the *NSF2*$^{E/Q}$ allele. The convergence of these independent data sets leads to the conclusion that F-actin is disrupted in the nerve terminal of the *NSF* alleles, and we suggest that this is a major factor contributing to the *NSF2* mutant phenotypes.

We have previously reported on diverse neural phenotypes associated with *NSF2*$^{E/Q}$ expression that include physiological and developmental perturbation (Stewart *et al.*, 2002, 2005). The present finding of F-actin disruption helps to reconcile the previous observations. The reduction in vesicle mobility, which we link to the reduced amount of F-actin, is consistent with the reduction in vesicle pool size and synaptic strength that we previously described (see also Cole *et al.*, 2000). Additionally, the hypersprouting phenotype is also consistent with a reduction in F-actin because *Drosophila* NMJs show hypersprouting when LIM kinase is down-regulated (Ang *et al.*, 2006) and mammalian neurons show greater neurite extension when actin dynamics are perturbed by increasing the activity of ADF/cofilin, an F-actin–depolymerizing factor (Endo *et al.*, 2003). Therefore, despite the apparent divergence of some of our earlier observations, these can now be explained by the unifying observation that disruption of F-actin in the *NSF2*$^{E/Q}$ allele underlies both the physiological and developmental phenotypes.

What is the relationship between NSF and actin? Because NSF is likely involved in many SNARE-dependent vesicular trafficking steps, one possibility is that manipulation of NSF simply impairs delivery of a cargo to the plasma membrane that is required for correct actin biochemistry and this then leads to the phenotypes we observe. Two pieces of evidence argue against this possibility. First, among SNARE-related genes the NMJ overgrowth phenotype is specific to *NSF2* alleles; mutation in either of the *Drosophila* SNAREs *Syntaxin 1A* or *n-Synaptobrevin*, which also dramatically impair neurotransmitter release, do not cause NMJ overgrowth (Stewart *et al.*, 2000), whereas $NSF2^{55}$ loss-of-function and $NSF2^{E/Q}$ alleles do (Stewart *et al.*, 2002, 2005). Second, mutations in *Drosophila kinesin*, which globally reduce vesicle traffic to the nerve terminal, do not cause NMJ overgrowth but rather they have reduced NMJ morphology (Hurd and Saxton, 1996). Therefore, these examples are not consistent with a general reduction in vesicle trafficking leading to *NSF*-like phenotypes. An alternative possibility is that NSF is involved, solely or with molecular partners, in regulating actin polymerization. There has been no previous finding of a direct biochemical interaction between NSF and actin, so it therefore seems more likely that the chaperone-like activity of NSF may regulate an upstream actin-regulatory or -stabilizing protein. The recent report of physical interaction between betaPix and NSF (Martin *et al.*, 2006) suggests a novel pathway linking NSF to p21-activated kinase (PAK) regulated actin dynamics. Interestingly, actin biochemistry is also disturbed in a temperature-sensitive *NSF* allele in *Dictyostelium* (Thompson and Bretscher, 2002), indicating the relationship between actin and NSF is not unique to our particular mutations.

Effects of Swinholide and Latrunculin

We found that both latrunculin and swinholide effectively dispersed the presynaptic actin-GFP puncta and that neither had an effect on the localization of synaptic vesicles. When we measured vesicle mobility we found reduced mobility in the treated boutons. Somewhat surprisingly we found that latrunculin partially restored mobility in the mutant line, whereas swinholide had no effect. We think that this result can be explained by the differing modes of action of these drugs. Although they both affect F-actin, they do so in different ways: Swinholide is an actin-severing agent that cuts actin filaments and stabilizes actin dimers, whereas latrunculin sequesters actin monomers and F-actin depolymerizes under endogenous actin cycling (Bubb *et al.*, 1995; Spector *et al.*, 1999; Fenteany and Zhu, 2003). It therefore seems likely that latrunculin cannot affect stable actin filaments, whereas swinholide should affect both stable and cycling actin. Therefore, the ability of latrunculin to partially restore vesicle mobility in the mutant is likely linked to its G-actin buffering capability. Because our actin-GFP FRAP data indicates that there is more G-actin within the $NSF2^{E/Q}$ boutons, application of latrunculin would remove the excess G-actin and potentially free some vesicular/actin interaction sites, allowing the vesicles to move upon available, albeit reduced, actin filaments. We currently do not know the nature of the interaction sites, but these could be provided by vesicle-associated myosin, for example.

Altogether our data indicate that NSF may play a central role in vesicular trafficking not only through its energetic disassembly of SNARE complexes, but also by fine-tuning the actin cytoskeleton. Future studies aimed at determining the molecular interactions between NSF and the signaling pathways that regulate actin will greatly inform us about the expanding role of NSF in vesicular trafficking.

ACKNOWLEDGMENTS

We thank L. Pallanck and D. Kiehart for providing fly stocks, N. Reist for anti-synaptotagmin antibodies, and Jingguo Ma and Sara Seabrooke for technical assistance. This work was financially supported by grants from Canadian Institutes for Health Research, Natural Sciences and Engineering Research Council of Canada, and a Premier's Research Excellence Award and the Canada Research Chairs Program to B.A.S.

REFERENCES

Ang, L. H., Chen, W., Yao, Y., Ozawa, R., Tao, E., Yonekura, J., Uemura, T., Keshishian, H., and Hing, H. (2006). Lim kinase regulates the development of olfactory and neuromuscular synapses. Dev. Biol. *293*, 178–190.

Bernstein, B. W., DeWit, M., and Bamburg, J. R. (1998). Actin disassembles reversibly during electrically induced recycling of synaptic vesicles in cultured neurons. Mol. Brain Res. *53*, 236–250.

Block, M. R., Glick, B. S., Wilcox, C. A., Wieland, F. T., and Rothman, J. E. (1988). Purification of an N-ethylmaleimide-sensitive protein catalyzing vesicular transport. Proc. Natl. Acad. Sci. USA *85*, 7852–7856.

Boulianne, G. L., and Trimble, W. S. (1995). Identification of a second homolog of N-ethylmaleimide-sensitive fusion protein that is expressed in the nervous system and secretory tissues of *Drosophila.* Proc. Natl. Acad. Sci. USA *92*, 7095–7099.

Bubb, M. R., Spector, I., Bershadsky, A. D., and Korn, E. D. (1995). Swinholide—A microfilament disrupting marine toxin that stabilizes actin dimers and severs actin-filaments. J. Biol. Chem. *270*, 3463–3466.

Cole, J. C., Villa, B. R., and Wilkinson, R. S. (2000). Disruption of actin impedes transmitter release in snake motor terminals. J. Physiol. *525*(Pt 3), 579–586.

Cong, M., Perry, S. J., Hu, L. A., Hanson, P. I., Claing, A., and Lefkowitz, R. J. (2001). Binding of the beta2 adrenergic receptor to N-ethylmaleimide-sensitive factor regulates receptor recycling. J. Biol. Chem. *276*, 45145–45152.

Doussau, F., and Augustine, G. J. (2000). The actin cytoskeleton and neurotransmitter release: an overview. Biochimie *82*, 353–363.

Dunaevsky, A., and Connor, E. A. (2000). F-actin is concentrated in nonrelease domains at frog neuromuscular junctions. J. Neurosci. *20*, 6007–6012.

Edwards, K. A., Demsky, M., Montague, R. A., Weymouth, N., and Kiehart, D. P. (1997). GFP-moesin illuminates actin cytoskeleton dynamics in living tissue and demonstrates cell shape changes during morphogenesis in *Drosophila.* Dev. Biol. *191*, 103–117.

Endo, M., Ohashi, K., Sasaki, Y., Goshima, Y., Niwa, R., Uemura, T., and Mizuno, K. (2003). Control of growth cone motility and morphology by LIM kinase and Slingshot via phosphorylation and dephosphorylation of cofilin. J. Neurosci. *23*, 2527–2537.

Estes, P. S., Ho, G. L., Narayanan, R., and Ramaswami, M. (2000). Synaptic localization and restricted diffusion of a *Drosophila* neuronal synaptobrevin–green fluorescent protein chimera in vivo. J. Neurogenet. *13*, 233–255.

Fenteany, G., and Zhu, S. T. (2003). Small-molecule inhibitors of actin dynamics and cell motility. Curr. Topics Med. Chem. *3*, 593–616.

Fleet, D. J., and Weiss, Y. (2005). Optical flow estimation. In: Mathematical Models for Computer Vision: The Handbook, ed. O. Faugeras, New York: Springer, 239–258.

Godenschwege, T. A., *et al.* (2004). Flies lacking all synapsins are unexpectedly healthy but are impaired in complex behaviour. Eur. J. Neurosci. *20*, 611–622.

Golby, J. A., Tolar, L. A., and Pallanck, L. (2001). Partitioning of N-ethylmaleimide-sensitive fusion (NSF) protein function in *Drosophila melanogaster*: dNSF1 is required in the nervous system, and dNSF2 is required in mesoderm. Genetics *158*, 265–278.

Han, S. Y., Park, D. Y., Park, S. D., and Hong, S. H. (2000). Identification of Rab6 as an N-ethylmaleimide-sensitive fusion protein-binding protein. Biochem. J. *352*(Pt 1), 165–173.

Henkel, A. W., Simpson, L. L., Ridge, R. M., and Betz, W. J. (1996). Synaptic vesicle movements monitored by fluorescence recovery after photobleaching in nerve terminals stained with FM1-43. J. Neurosci. *16*, 3960–3967.

Hilfiker, S., Benfenati, F., Doussau, F., Nairn, A. C., Czernik, A. J., Augustine, G. J., and Greengard, P. (2005). Structural domains involved in the regulation of transmitter release by synapsins. J. Neurosci. *25*, 2658–2669.

Holt, M., Cooke, A., Neef, A., and Lagnado, L. (2004). High mobility of vesicles supports continuous exocytosis at a ribbon synapse. Curr. Biol. *14*, 173–183.

Hurd, D. D., and Saxton, W. M. (1996). Kinesin mutations cause motor neuron disease phenotypes by disrupting fast axonal transport in *Drosophila*. Genetics *144*, 1075–1085.

Kawasaki, F., Mattiuz, A. M., and Ordway, R. W. (1998). Synaptic physiology and ultrastructure in comatose mutants define an in vivo role for NSF in neurotransmitter release. J. Neurosci. *18*, 10241–10249.

Koh, T. W., Verstreken, P., and Bellen, H. J. (2004). Dap160/intersectin acts as a stabilizing scaffold required for synaptic development and vesicle endocytosis. Neuron *43*, 193–205.

Kraszewski, K., Daniell, L., Mundigl, O., and DeCamilli, P. (1996). Mobility of synaptic vesicles in nerve endings monitored by recovery from photobleaching of synaptic vesicle–associated fluorescence. J. Neurosci. *16*, 5905–5913.

Kuromi, H., and Kidokoro, Y. (1998). Two distinct pools of synaptic vesicles in single presynaptic boutons in a temperature-sensitive *Drosophila* mutant, shibire. Neuron *20*, 917–925.

Laviolette, M. J., Nunes, P., Peyre, J. B., Aigaki, T., and Stewart, B. A. (2005). A genetic screen for suppressors of *Drosophila* NSF2 neuromuscular junction overgrowth. Genetics *170*, 779–792.

Martin, H. G., Henley, J. M., and Meyer, G. (2006). Novel putative targets of N-ethylmaleimide sensitive fusion protein (NSF) and alpha/beta soluble NSF attachment proteins (SNAPs) include the Pak-binding nucleotide exchange factor betaPIX. J. Cell. Biochem., 10.100/jcb.20998.

McDonald, P. H., Cote, N. L., Lin, F. T., Premont, R. T., Pitcher, J. A., and Lefkowitz, R. J. (1999). Identification of NSF as a beta-arrestin1-binding protein. Implications for beta2-adrenergic receptor regulation. J. Biol. Chem. *274*, 10677–10680.

Merrifield, C. J., Moss, S. E., Ballestrem, C., Imhof, B. A., Giese, G., Wunderlich, I., and Almers, W. (1999). Endocytic vesicles move at the tips of actin tails in cultured mast cells. Nat. Cell Biol. *1*, 72–74.

Morales, M., Colicos, M. A., and Goda, Y. (2000). Actin-dependent regulation of neurotransmitter release at central synapses. Neuron *27*, 539–550.

Muller, J. M., Shorter, J., Newman, R., Deinhardt, K., Sagiv, Y., Elazar, Z., Warren, G., and Shima, D. T. (2002). Sequential SNARE disassembly and GATE-16-GOS-28 complex assembly mediated by distinct NSF activities drives Golgi membrane fusion. J. Cell Biol. *157*, 1161–1173.

Nishimune, A., Isaac, J. T., Molnar, E., Noel, J., Nash, S. R., Tagaya, M., Collingridge, G. L., Nakanishi, S., and Henley, J. M. (1998). NSF binding to GluR2 regulates synaptic transmission. Neuron *21*, 87–97.

Pallanck, L., Ordway, R. W., Ramaswami, M., Chi, W. Y., Krishnan, K. S., and Ganetzky, B. (1995). Distinct roles for N-ethylmaleimide-sensitive fusion protein (NSF) suggested by the identification of a second *Drosophila* NSF homolog. J. Biol. Chem. *270*, 18742–18744.

Richards, D. A., Guatimosim, C., and Betz, W. J. (2000). Two endocytic recycling routes selectively fill two vesicle pools in frog motor nerve terminals. Neuron *27*, 551–559.

Richards, D. A., Rizzoli, S. O., and Betz, W. J. (2004). Effects of wortmannin and latrunculin A on slow endocytosis at the frog neuromuscular junction. J. Physiol. *557*, 77–91.

Rosahl, T. W., Spillane, D., Missler, M., Herz, J., Selig, D. K., Wolff, J. R., Hammer, R. E., Malenka, R. C., and Sudhof, T. C. (1995). Essential functions of synapsins I and II in synaptic vesicle regulation. Nature *375*, 488–493.

Sakaba, T., and Neher, E. (2003). Involvement of actin polymerization in vesicle recruitment at the calyx of Held synapse. J. Neurosci. *23*, 837–846.

Sankaranarayanan, S., Atluri, P. P., and Ryan, T. A. (2003). Actin has a molecular scaffolding, not propulsive, role in presynaptic function. Nat. Neurosci. *6*, 127–135.

Shupliakov, O., Bloom, O., Gustafsson, J. S., Kjaerulff, O., Low, P., Tomilin, N., Pieribone, V. A., Greengard, P., and Brodin, L. (2002). Impaired recycling of synaptic vesicles after acute perturbation of the presynaptic actin cytoskeleton. Proc. Natl. Acad. Sci. USA *99*, 14476–14481.

Sollner, T., Bennett, M. K., Whiteheart, S. W., Scheller, R. H., and Rothman, J. E. (1993a). A protein assembly-disassembly pathway in vitro that may correspond to sequential steps of synaptic vesicle docking, activation, and fusion. Cell *75*, 409–418.

Sollner, T., Whiteheart, S. W., Brunner, M., Erdjument-Bromage, H., Geromanos, S., Tempst, P., and Rothman, J. E. (1993b). SNAP receptors implicated in vesicle targeting and fusion. Nature *362*, 318–324.

Song, I., Kamboj, S., Xia, J., Dong, H., Liao, D., and Huganir, R. L. (1998). Interaction of the N-ethylmaleimide-sensitive factor with AMPA receptors. Neuron *21*, 393–400.

Spector, I., Braet, F., Shochet, N. R., and Bubb, M. R. (1999). New anti-actin drugs in the study of the organization and function of the actin cytoskeleton. Microsc. Res. Tech. *47*, 18–37.

Stewart, B. A., Atwood, H. L., Renger, J. J., Wang, J., and Wu, C. F. (1994). Improved stability of *Drosophila* larval neuromuscular preparations in haemolymph-like physiological solutions. J. Comp. Physiol. A *175*, 179–191.

Stewart, B. A., Mohtashami, M., Rivlin, P., Deitcher, D. L., Trimble, W. S., and Boulianne, G. L. (2002). Dominant-negative NSF2 disrupts the structure and function of *Drosophila* neuromuscular synapses. J. Neurobiol. *51*, 261–271.

Stewart, B. A., Mohtashami, M., Trimble, W. S., and Boulianne, G. L. (2000). SNARE proteins contribute to calcium cooperativity of synaptic transmission. Proc. Natl. Acad. Sci. USA *97*, 13955–13960.

Stewart, B. A., Mohtashami, M., Zhou, L., Trimble, W. S., and Boulianne, G. L. (2001). SNARE-dependent signaling at the *Drosophila* wing margin. Dev. Biol. *234*, 13–23.

Stewart, B. A., Pearce, J., Bajec, M. R., and Khorana, R. (2005). Disruption of synaptic development and ultrastructure by *Drosophila* NSF2 alleles. J. Comp. Neurol. *488*, 101–111.

Thompson, C. R., and Bretscher, M. S. (2002). Cell polarity and locomotion, as well as endocytosis, depend on NSF. Development *129*, 4185–4192.

Verstreken, P., Kjaerulff, O., Lloyd, T. E., Atkinson, R., Zhou, Y., Meinertzhagen, I. A., and Bellen, H. J. (2002). Endophilin mutations block clathrin-mediated endocytosis but not neurotransmitter release. Cell *109*, 101–112.

Verstreken, P., Koh, T. W., Schulze, K. L., Zhai, R. G., Hiesinger, P. R., Zhou, Y., Mehta, S. Q., Cao, Y., Roos, J., and Bellen, H. J. (2003). Synaptojanin is recruited by endophilin to promote synaptic vesicle uncoating. Neuron *40*, 733–748.

Wang, X. H., Zheng, J. Q., and Poo, M. M. (1996). Effects of cytochalasin treatment on short-term synaptic plasticity at developing neuromuscular junctions in frogs. J. Physiol. *491*, 187–195.

Whiteheart, S. W., Brunner, M., Wilson, D. W., Wiedmann, M., and Rothman, J. E. (1992). Soluble N-ethylmaleimide-sensitive fusion attachment proteins (SNAPs) bind to a multi-SNAP receptor complex in Golgi membranes. J. Biol. Chem. *267*, 12239–12243.

Whiteheart, S. W., Rossnagel, K., Buhrow, S. A., Brunner, M., Jaenicke, R., and Rothman, J. E. (1994). N-ethylmaleimide-sensitive fusion protein: a trimeric ATPase whose hydrolysis of ATP is required for membrane fusion. J. Cell Biol. *126*, 945–954.

Xu, Z., Sato, K., and Wickner, W. (1998). LMA1 binds to vacuoles at Sec18p (NSF), transfers upon ATP hydrolysis to a t-SNARE (Vam3p) complex, and is released during fusion. Cell *93*, 1125–1134.

Zhang, B., Koh, Y. H., Beckstead, R. B., Budnik, V., Ganetzky, B., and Bellen, H. J. (1998). Synaptic vesicle size and number are regulated by a clathrin adaptor protein required for endocytosis [In Process Citation]. Neuron *21*, 1465–1475.

Zhang, Y. Q., Rodesch, C. K., and Broadie, K. (2002). Living synaptic vesicle marker: synaptotagmin-GFP. Genesis *34*, 142–145.